

RADIATIVE TRANSITIONS IN STRONGLY COUPLED LASER-GENERATED PLASMAS

H. B. Nersisyan,^{1,2,*} C. Toepfffer,² and H. H. Matevosyan¹

¹Laboratory of Theoretical Physics, Institute of Radiophysics and Electronics, Ashtarak, Armenia

²Institut für Theoretische Physik II, Universität Erlangen-Nürnberg, Staudtstr. 7, D-91058 Erlangen, Germany

Received 10 October, 2008

Abstract

The spectral line shapes for hydrogen-like heavy ion emitters embedded in strongly correlated two-component electron-ion plasmas are investigated with numerical simulations. For that purpose the microfield fluctuations are calculated by molecular dynamics simulations where short range quantum effects are taken into account by using a regularized Coulomb potential for the electron-ion interaction. The microfield fluctuations are used as input in a numerical solution of the time-dependent Schrödinger equation for the radiating electron. In distinction to the standard impact and quasistatic approximations the method presented here allows to account for the correlations between plasma ions and electrons. The shape of the Ly_α-line in Al is investigated in the intermediate regime. The calculations are in good agreement with experiments on the Ly_α-line in laser generated Al plasmas.

PACS numbers: 32.30.Rj; 32.70.Jz; 52.25.Os; 52.65.Yy

Keywords: X-ray spectra; line broadening; strongly coupled plasmas; molecular dynamics simulations

I. INTRODUCTION

Because of the rapid progress of technology [1] previously unaccessible states of matter can be investigated by irradiation with powerful lasers. A few typical examples are the compression of deuterium pellets for inertial fusion [2, 3] and shock wave experiments to investigate possible phase transitions like the metallization of hydrogen [4], which are not only of large fundamental interest [5] but also important for astrophysical problems like the structure of the giant planets [6]. Such experiments require typically large lasers delivering pulses with PW power for $1-10^3$ ps.

In comparison to isolated atoms or ions the interactions within a plasma shift and distort the spectral lines corresponding to radiative transitions. Spectroscopy is therefore a tool to diagnose the state of a plasma. The fluctuations of the electric microfield $\mathbf{E}(t)$ are of particular relevance. For the shape of the spectral lines two frequencies are important. These are: a field frequency $\omega_0 = |\dot{\mathbf{E}}(t)/\mathbf{E}(t)|$ characterizing the fluctuations of the perturbing field and the splitting of spectral lines $\Delta\omega$ due to the Stark effect. The calculation of line shapes is facilitated by approximations which are valid in complementary extreme regimes [7]. If the shortest time scale is set by ω_0 , the radiator is perturbed by a set of instantaneous collisions which need not be further resolved in time. This impact approximation is often valid to describe the perturbations due to swiftly moving plasma electrons. However, if the shortest time scale is set by $\Delta\omega$, it is only the probability distribution $P(E)$ of the electric field which matters. This quasi-static approximation is usually employed to account for the influence of the heavier, slowly moving plasma ions. Moreover, if the electric microfields are sufficiently weak, both $P(E)$ and the Stark splitting $\Delta\omega$ can be calculated perturbatively.

In the intermediate regime approximations have been proposed which generally involve several assumptions and idealizations. They should therefore be regarded as model calculations. Formerly, the hopes for a truly unified and practical theory were considered as dim [7]. In the meantime progress has been made by treating the effect of the ions on the radiator in an effective independent-particle model (APEX) [8–10] as well as the Coulomb interaction between the electrons and the radiator beyond the dipole term [11]. These methods were applied to highly charged Ar ions in D plasmas [11–13]. In the present paper we want to study even stronger coupled systems, e.g. highly charged radiators in plasmas with highly charged ions. For that purpose we perform numerical simulations which cover a wide range of plasma densities and temperatures accessible in present experiments or in the near future. The simulations span the entire range between the impact and the quasi-static approximations. We explicitly solve the time-dependent Schrödinger equation for the radiator in the fluctuating microfield generated by the other plasma particles. As we want to account for strong correlations in the plasma, the microfield fluctuations are obtained from molecular dynamics (MD) simulations.

The paper is organized as follows. In Sec. II we present the calculation of the actual fluctuating microfield by MD simulations. In Sec. III we describe the radiating ion and its coupling to the electric microfield. In Sec. IV we calculate the shape of the Ly_α-lines in aluminum two-component plasmas for a wide range of plasma densities and the regularization parameter. We compare our calculations with experiments performed in Garching [14–16]. As shown in [17, 18] these experiments already reached plasma regimes where the traditional approximations, impact for the electrons and quasi-static for the ions, cease to be valid.

*Also at Centre of Strong Fields Physics, Yerevan State University,
Alex Manoogian st. 1, Yerevan, Armenia. E-mail: hrachya@iprhe.am

II MD SIMULATIONS OF PLASMA MICROFIELDS

A two-component plasma (TCP) of electrons and ions (with the charge Ze) is in equilibrium with the temperature T completely described by the coupling parameters $\Gamma_{\alpha\beta}$ with $\alpha, \beta = e, i$. Introducing the Wigner-Seitz radii, i.e., the mean electron-electron, electron-ion, and ion-ion distances through the relations, $\alpha_e^{-3} = 4\pi n_e/3$, $\alpha_i^{-3} = 4\pi n_i/3$, and $\alpha_{ii}^{-3} = 4\pi n_i/3$, where $n = n_e + n_i$ is the total plasma density with $n_e = Zn_i$) these parameters are defined as [19-21]

$$\Gamma_{ee} = \frac{e_s^2}{a_e k_B T}, \quad \Gamma_{ei} = \frac{Ze_s^2}{ak_B T}, \quad \Gamma_{ii} = \frac{Z^2 e_s^2}{a_e k_B T}, \quad (1)$$

respectively. Here $e_s^2 = e^2/4\pi\epsilon_0$, and ϵ_0 is the permittivity of the vacuum. Note that

$$\Gamma_{ee} = \frac{\Gamma_{ei}}{\left[Z^2(Z+1)\right]^{1/3}}, \quad \Gamma_{ii} = \frac{Z\Gamma_{ee}}{(Z+1)^{1/3}}, \quad (2)$$

In a hydrogen plasma with $Z = 1$ we obtain $\Gamma_{ee} = \Gamma_{ii} = 2^{-1/3}\Gamma_{ei}$ while in a plasma with highly charged ions ($Z \gg 1$) $\Gamma_{ii} = Z^{2/3}\Gamma_{ei}$ and $\Gamma_{ee} = \Gamma_{ei}/Z$. For $Z \geq 2$ the coupling parameters satisfy the inequality $\Gamma_{ee} < \Gamma_{ei} < \Gamma_{ii}$.

Here we consider the hydrogen-like radiator with the charge $(Z_R - 1)e$ and the pair interaction potential $e_s^2 q_\alpha q_\beta u_{\alpha\beta}(r)$ with $\alpha, \beta = e, i, R$ (throughout this paper the index R refers to the radiators), $q_e = -1$, $q_i = Z$, $q_R = Z_R - 1$, and

$$u_{\alpha\beta}(r) = \frac{1}{r} \left(1 - e^{-r/\delta_{\alpha\beta}}\right) \quad (3)$$

which is regularized at small distances due to quantum diffraction effects. In this paper we assume that the Coulomb potential is cut-off at the distances $\delta_{\alpha\beta}$ which are related to the thermal de Broglie wavelengths, $\delta_{\alpha\beta} = (2\pi\hbar^2/\mu_{\alpha\beta} k_B T)^{1/2}$, where $\mu_{\alpha\beta}$ is the reduced mass of the particles α and β . For large distances $r > \delta_{\alpha\beta}$ the potential becomes Coulomb, while for $r < \delta_{\alpha\beta}$ the Coulomb singularity is removed and $u_{\alpha\beta}(0) = 1/\delta_{\alpha\beta}$. By this the short-range effects based on the uncertainty principle are included [22-25].

For a classical description of a plasma the electron degeneracy parameter Θ_e , i.e., the ratio of the thermal energy and the Fermi energy must fulfill $\Theta_e = k_B T/E_F > 1$. Or, alternatively, the electron thermal wavelength should be smaller than the electron-electron mean distance, $\delta_{ee} < 2(16\pi/81)^{1/6} a_e \approx 1.85 a_e$. Since an ion is much heavier than an electron this condition is usually fulfilled for ions. We note that $\delta_{ii} \ll \delta_{ei}$ and $\delta_{ee} \simeq 2^{1/2}\delta_{ei}$ since $\mu_{ei} \simeq m$. Therefore one can expect that the regularization given by Eq. (3) is less important for ions than for electrons. Furthermore, scattering of any two particles is classical for impact parameters that are large compared to the de Broglie wavelengths. Typical impact parameters are given by the Landau lengths, $\lambda_{La\beta} = e_s^2 |q_\alpha q_\beta|/k_B T$. Its ratio to the de Broglie wavelengths is given by

$$\sigma_{\alpha\beta} = \frac{\lambda_{La\beta}}{\delta_{\alpha\beta}} = \frac{\Gamma_{ei} |q_\alpha q_\beta|}{Z} \frac{a}{\delta_{\alpha\beta}} = \frac{e_s^2 |q_\alpha q_\beta| u_{\alpha\beta}(0)}{(2\pi)^{1/2} k_B T}. \quad (4)$$

This is also the maximum value of the interparticle interaction energy in the units of $k_B T$, where $\sigma_{ee} < \sigma_{ei} \ll \sigma_{ii}$ and $\sigma_{ei} \simeq 2^{1/2}Z\sigma_{ee}$. A classical description of the scattering events in the TCP is valid if $\sigma ee > 1$.

A collective length scale is given by the Debye screening radius, for a TCP $\lambda_D = a (3\Gamma_{ei})^{-1/2}$. The plasma frequencies for electrons and ions $\omega_{pa} = (4\pi q_a n \alpha e_s^2 / m_a)^{1/2}$ with $\alpha = e, i$ set the collective time scales ω_{pe}^{-1} and ω_{pi}^{-1} for electronic and ionic subspecies, respectively. Moreover, for a nonrelativistic treatment the thermal energy of the particles must be smaller than their rest energy. Since this is important only for electrons we require that $k_B T \ll mc^2$. Also the validity of the dipole approximation for plasma-radiator interaction used in Sec. III (see Eq. (7) below) requires that the characteristic length scale of the plasma microfield must be larger than the effective atomic length scale $a_Z = a_B/Z$, where $a_B = \hbar^2/me_s^2$ is the Bohr radius. Since this length is $\simeq a$ the dipole approximation is valid when the mean distance a between the particles is larger than a_Z which is usually fulfilled for heavy radiators. We consider hydrogen-like ions as radiators in a completely ionized TCP. Due to their large mass ratio the electrons and the ions move on very different timescales. In contrast to Refs. [17, 18] we treat here the ions and electrons on an equal footing by concentrating on the TCP.

As discussed above the electric microfield distribution (MFD) $P(E)$ plays a central role for the line shape. Models for this distribution exist in the limits of an ideal plasma [26], a weakly coupled plasma [27] and for very strongly coupled plasmas [28]. For intermediate cases an effective independent-particle model

known as Adjustable Parameter Exponential (APEX) approximation has been developed in [8–10] for an ionic one-component plasma (OCP). It rests essentially on the pair distribution function and has been tested by comparison with MD and Monte-Carlo simulations. Recently in Refs. [19–21] we have suggested two theoretical models named PMFEX and PMFEX+ (Potential of Mean Force Exponential approximation) which turn out to be a very reliable approaches for calculating the MFD of a TCP with attractive interaction. In order to cover the entire range from small to large plasma parameters, we use here classical MD simulations which have been described in detail in Refs. [19–21, 29]. As an example the normalized MFDs from PMFEX and MD are compared in Fig. 1 where the electric microfields are scaled in units of the Holtsmark field E_H for a TCP (see [19] for details)

$$E_H = \frac{C\mathcal{Z}e}{4\pi\epsilon_0 a^2}, \quad \mathcal{Z} = \left[\frac{Z(1+Z^{1/2})}{Z+1} \right]^{2/3}, \quad (5)$$

with an effective charge \mathcal{Z} and $C = (8\pi/25)^{1/3}$. For a hydrogen TCP with $Z = 1$ also $\mathcal{Z} = 1$. In other cases the effective charge increases with Z and behaves as $\mathcal{Z} \approx Z^{1/3}$ for large Z . Thus the ideal two-component plasma can be regarded as an ionic OCP with effective ionic charge Z . These distributions were obtained from ensembles of fields taken at a charged reference point which is chosen to be one of the plasma ions.

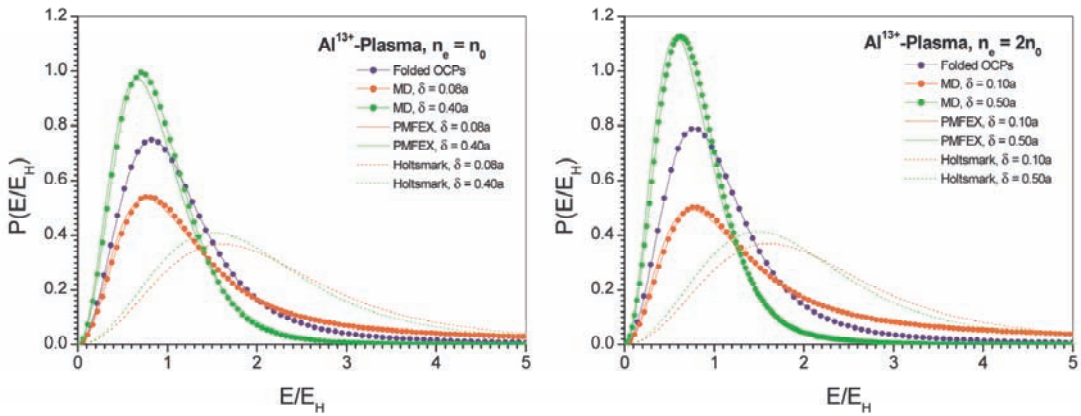


FIG. 1: Normalized MFD for Al^{13+} TCPs with $k_B T = 500$ eV, $n_e = n_0$, $\Gamma_{ee} = 0.037$, $\Gamma_{ii} = 2.65$ (left) and $n_e = 2n_0$, $\Gamma_{ee} = 0.046$, $\Gamma_{ii} = 3.34$ (right) as a function of the electric field in units of E_H , Eq. (5), for different values of δ . The lines with and without symbols represent the MFD from the MD simulations and PMFEX model, respectively. The blue lines with circles are the MFD obtained from the folding of an electronic and an ionic OCP, see Eq. (6). The Holtsmark distributions for a TCP are shown as dashed lines.

The MFDs for Al^{13+} two-component plasmas with temperature $k_B T = 500$ eV and with coupling parameters $\Gamma_{ee} = 0.037$, $\Gamma_{ii} = 2.65$ and $\Gamma_{ee} = 0.046$, $\Gamma_{ii} = 3.34$ are shown in left and right panels of Fig. 1, respectively, for different values of $\delta_{ei} = \delta$. In both cases $\delta_{ee} \approx 0$, $\delta_{ii} \approx 0$. The density of plasma electrons is measured in units of $n_0 = 5 \times 10^{23} \text{ cm}^{-3}$. The dashed curves are, for comparison, the Holtsmark MFDs for a TCP with regularized Coulomb potential. Here these MFDs depend on Z and δ as discussed in [19]. To demonstrate the importance of the attractive interactions we also plotted the MFDs $P_0(E)$ resulting from the corresponding electronic and ionic OCPs with Γ_{ee} and Γ_{ii} , respectively (blue lines with circles). To that end the distribution $Q_0(E) = P_0(E)/(4\pi E^2)$ of the total field $\mathbf{E} = \mathbf{E}_1 + \mathbf{E}_2$ is calculated as

$$Q_0(E) = \int d\mathbf{E}_1 d\mathbf{E}_2 \delta(\mathbf{E} - \mathbf{E}_1 - \mathbf{E}_2) Q_e(\mathbf{E}_1) Q_i(\mathbf{E}_2) \quad (6)$$

from the MFD of the ionic OCP at a charged point $Q_i(E_2)$ and of the electronic OCP at a neutral reference point $Q_e(E_1)$. The distribution $Q_0(E)$ thus represents the MFD in a TCP assuming that the ion-electron attractive interaction is switched off. Here $Q_e(E_1)$ and $Q_i(E_2)$ are taken from MD simulations of an OCP. As the thermal motion of the particles is suppressed with increasing coupling the distributions $P(E)$ and the mean electric fields are shifted towards smaller values as shown in Fig. 1. This figure also shows the importance of the attractive interactions in plasmas. The behavior of the MFD with respect to the variation of the parameter δ is particularly noteworthy. For fixed coupling parameters the maximum of the MFD shifts only slightly to lower field strengths E with increasing δ (see Fig. 1) while the maximum itself increases with δ . This is related to the largest possible single-particle field $|E_e(0)| = e/(8\pi\epsilon_0\delta^2)$, which an electron can produce at the ion. Thus the nearest neighbor electronic MFD vanishes for electric fields larger than $|E_e(0)|$, and smaller δ will result in larger contributions to $P(E)$ at higher fields E with a corresponding reduction of $P(E)$ at small fields. Therefore, the formation of the tails in the MFD and

enhancement of the electric microfield at small δ may have important influence on the spectral line shapes of the radiating particles. Further examples for charged and neutral radiators, together with a detailed discussion of the limits of the PMFEX treatment at increasing coupling, are given in Refs. [19–21].

The time-dependent Schrödinger equation (see Eq. (11) below) describing the coupling of the microfield to the radiator is then solved for an ensemble of typically thirty independent microfields. This yields the mean emission as well as the statistical error (mean error to the mean). Finally, we note that our MD simulations provide the data for the electric microfield $\mathbf{E}(t)$ only on the radiator with the total charge $Z_R - 1 = Z$ or $Z_R - 1 = 0$. This restricts the possible type of the radiating hydrogen-like radiator. Indeed this approach allows either neutral hydrogen H^0 embeded in a H^{+} -TCP or any other hydrogen-like heavy ion $A^{(Z-1)+}$ with the total charge $Z - 1 \approx Z$ embedded in a A^{Z+} -TCP. Obviously for heavy ions with $Z \gg 1$ one can neglect the difference between the Coulomb coupling strengths of $A^{(Z-1)+}$ and A^{Z+} radiators to the plasma.

III. WAVE EQUATION FOR A HYDROGENLIKE ION IN A TIME-DEPENDENT ELECTRIC FIELD

In this section we describe the solution of the wave equation for a hydrogen-like ion coupled to the timedeependent electric microfield. The microfield fluctuations in the plasma are calculated by the MD simulations as discussed in Sec. II. We consider a hydrogen-like ion in a time-dependent electric microfield. The Hamiltonian is the sum of \hat{H}_0 describing the unperturbed ion and a dipole term $\hat{H}_{\text{int}} = e\mathbf{r}\cdot\mathbf{E}(t)$ for the interaction between the bound electron (charge $-e$, distance \mathbf{r} from nucleus) and the microfield $\mathbf{E}(t)$,

$$\hat{H} = \hat{H}_0 + \hat{H}_{\text{int}} \quad (7)$$

The electron with mass m moves in the potential of a nucleus with charge $Z_R e$. In the present application it turns out that it suffices to start from the non-relativistic Schrödinger equation

$$\hat{H}_0 |\alpha\rangle = \left(\frac{\hat{\mathbf{p}}^2}{2m} - \frac{Z_R e_s^2}{r} \right) |\alpha\rangle = \hbar\omega_\alpha |\alpha\rangle \quad (8)$$

for the time-independent electronic state $|\alpha\rangle$ with energy $E_\alpha = \hbar\omega_\alpha$. Here $\hat{\mathbf{p}}$ is the momentum operator and α is a multiindex including radial, angular momentum and spin quantum numbers. The present calculations are done in the configuration space corresponding to the solutions of Eq. (8). In order to discretize the continuum, a boundary condition $\langle \mathbf{r} | \alpha \rangle = 0$ is imposed at a radius $r = R_0$, which is chosen sufficiently large in order to avoid an influence on the final results. The radial wave functions with this boundary condition are still confluent hypergeometric functions, but the radial quantum numbers of bound states are not integers any more [17, 18]. In order to obtain a finite basis, the (former) continuum states are cut off at sufficiently large quantum numbers. Alternatively the continuum could be handled by forming wave packets with a width that must be adjusted appropriately [30]. In Refs. [17, 18] the time-dependent equation $\hat{H}\Psi(t) = i\hbar\Psi'(t)$ with the Hamiltonian (7) has also been solved on a grid for the electron wave function [31, 32]. This is more advantageous for the description of the continuum and it is easier to implement the interactions between the radiator and the plasma particles beyond the dipole term in Eq. (7). On the other hand, spatially extended states require very large simulation boxes. Quite generally in the present context the solution on the grid is more expensive numerically than working in configuration space (see discussions in Refs. [17, 18]). As in [17, 18] we adopted the latter for the subsequent calculations.

At high Z_R relativistic corrections must be considered and also the spin should be treated as a dynamical variable. It turns out that in the cases considered here it suffices to include the first-order fine-structure shift [33]

$$\Delta E_{nlj} = -\frac{Z_R^2 \alpha_s^2 |E_n|}{n} \left(\frac{1}{\gamma_{lj}} - \frac{3}{4n} \right), \quad (9)$$

where $\gamma_{lj} = j + 1/2$ and $\gamma_{lj} = 1$ at $l \geq 1$ and $l = 0$, respectively. Here n is the principal quantum number of the hydrogen-like ion, $|E_n| = -Z_R^2 E_B / n^2$ is the corresponding energy ($E_B = e_s^2 / 2a_B$ is the Bohr energy), $j = l \pm 1/2$ is the total angular momentum quantum number and $\alpha_s \approx 1/137$ is the Sommerfeld constant.

The dipole interaction $e\mathbf{r}\cdot\mathbf{E}(t)$ between the radiator and the plasma is time-dependent and possibly strong. Going beyond the second order treatment of Ref. [11] we use the interaction picture with the

unperturbed basis states given by Eq. (8). The time-dependent Schrödinger equation with the total Hamiltonian (7) can be solved using Dirac's method. The perturbed electron wave function is represented as a sum of wave functions of the unperturbed Hamiltonian with time-dependent coefficients $c_\alpha(t)$:

$$\Psi(t) = \sum_\alpha c_\alpha(t) e^{-i\omega_\alpha t} |\alpha\rangle. \quad (10)$$

A substitution of Eq. (10) into the time-dependent Schrödinger equation and orthogonality of the spatial wave functions, i.e., $\langle \alpha | \beta \rangle = \delta_{\alpha\beta}$, gives the set of coupled ordinary and linear differential equations

$$\dot{c}_\alpha(t) = -\frac{ie}{\hbar} \mathbf{E}(t) \cdot \sum_\beta e^{i\omega_{\alpha\beta} t} c_\beta(t) \langle \alpha | \mathbf{r} | \beta \rangle \quad (11)$$

which is solved iteratively. Here $\hbar\omega_{\alpha\beta}$ is the transition energy between atomic states α and β , i.e., $\omega_{\alpha\beta} = \omega_\alpha - \omega_\beta$. Within the dipole approximation the transition rate per unit time and energy interval $I(\omega)$ for the emission of photons is proportional to the power spectrum of the dipole operator [34]. It is defined as the square of the absolute value of the Fourier transform of the expectation value of the dipole operator. Hence we introduce

$$I(\omega) = \frac{2e_s^2 \omega^3}{3\pi c^3 \hbar^2 \tau} \left| \int_0^\tau \mathbf{d}(t) e^{i\omega t} dt \right|^2 \quad (12)$$

with $\tau \rightarrow \infty$ and the expectation value of the dipole moment

$$\mathbf{d}(t) = \sum_\beta e^{i\omega_{\beta\alpha} t} c_\beta^*(t) c_\alpha(t) \langle \beta | \mathbf{r} | \alpha \rangle. \quad (13)$$

Let us now consider a transition $\alpha \rightarrow g$ downwards to a state $|g\rangle$ which is nearly filled, i.e., $c_\beta(t) = \delta_{\beta_g}$.

Then the dipole moment in Eq. (13) is calculated with respect to the state $|g\rangle$ and

$$I(\omega) = \frac{2e_s^2 \omega^3}{3\pi c^3 \hbar^2 \tau} \left| \sum_\alpha \langle g | r | \alpha \rangle \int_0^\tau c_\alpha(t) e^{i(\omega - \omega_{\alpha g}) t} dt \right|^2 \quad (14)$$

Until now we have neglected the interaction $\hat{H}_{e\gamma}$ of the radiating electron with the emitted photons. In this case, as shown in Refs. [17, 18], the total radiated power given in Eq. (14) is underestimated for the excited radiators where $|c_g|^2 < 1$. This can be compensated by dividing through the time-averaged occupation probability of the lower state

$$I(\omega) \rightarrow \frac{I(\omega)}{\langle |c_g(t)|^2 \rangle_t} \quad (15)$$

The subsequent calculations will be done in this dipole power spectrum approximation (DPSA). The validity of this approximation has been tested in Refs. [17, 18] in the wide range of plasma and radiator parameters by comparing explicitly $I(\omega)$ with the spectrum obtained from the total Hamiltonian $\hat{H}' = \hat{H}_0 + \hat{H}_{\text{int}} + \hat{H}_{e\gamma}$. The DPSA is justified as the emission of radiation through the interaction $\hat{H}_{e\gamma}$ changes the occupation probabilities of the radiator's states on a much slower scale than the fluctuating electric microfields.

At this stage we have neglected the feedback of the radiator's excitation to the plasma. In this respect the plasma particles move as if they had an infinite mass. As they have a finite velocity it appears as if the radiating electron is embedded in a plasma of infinite temperature. Accordingly the time evolution of the total system will lead to an equal population of all electronic states. As the time-dependent feedback could be implemented only at a very great expense in the MD simulations we enforce a canonical equilibrium state of the plasma and the radiating electron by modifying the interaction in Eq. (11) according to

$$\mathbf{er} \cdot \mathbf{E}(t) \rightarrow e^{-\beta \hat{H}_0/2} \mathbf{er} \cdot \mathbf{E}(t) e^{\beta \hat{H}_0/2} \quad (16)$$

with $\beta = 1/k_B T$, where T is the plasma temperature.

IV. SIMULATION OF Ly _{α} -LINES AND COMPARISON WITH EXPERIMENT

Using the theoretical background introduced so far we present in this Section calculations of the shape of the Ly _{α} line of Al¹²⁺ radiating ion embedded in a Al¹³⁺-TCP in a wide range of plasma

parameters. The unperturbed transition energy for the Ly _{α} line is $\hbar\omega_{Ly\alpha} = (3/4)Z_R^2 E_B$ with $E_B \simeq 13.6$ eV. For instance, for hydrogen (H^0) and aluminum (Al^{12+}) radiators $\hbar\omega_{Ly\alpha} \simeq 10.2$ eV and $\hbar\omega_{Ly\alpha} \simeq 1724.5$ eV, respectively. However, as we have mentioned in Sec. III, for heavy ions the relativistic corrections, i.e. the fine structure of the levels must be accounted for. Using the fine structure shift in Eq. (9) the unperturbed Ly _{α} transition energy becomes

$$\hbar\omega_{Ly\alpha} = \frac{3}{4}Z_R^2 E_B \left(1 + CjZ_R^2 \alpha_s^2\right) \quad (17)$$

with $C_{1/2} = 11/48$, $C_{3/2} = 5/16$ and for Al^{12+} ions $\hbar\omega_{Ly\alpha} \simeq 1728.1$ eV and $\hbar\omega_{Ly\alpha} \simeq 1729.4$ eV with $j = 1/2$ and $j = 3/2$, respectively.

We start from the line as it is broadened by the Al^{13+} ions and electrons in the plasma. Then we fold with the weighted fine structure shift Eq. (9) which is $\hbar\Delta\omega \simeq 1.29$ eV according to

$$LS|I(\omega)| = \frac{1}{3}I\left(\omega + \frac{2}{3}\Delta\omega\right) + \frac{2}{3}I\left(\omega - \frac{1}{3}\Delta\omega\right) \quad (18)$$

and account for the Doppler effect [35] which broadens a line with the unperturbed frequency ω_0 according to a Gaussian distribution

$$L|\Delta\omega| = \frac{1}{\sqrt{2\pi}\sigma} \exp\left[-\frac{1}{2}\left(\frac{\Delta\omega}{\sigma}\right)^2\right], \quad (19)$$

where $\Delta\omega = \omega - \omega_0$ and

$$\sigma^2 = \frac{\omega_w^2}{8\ln 2} = \omega_0^2 \frac{k_B T}{M_R c^2} \quad (20)$$

Here $\hbar\omega_w$ is the full width at half maximum (FWHM) of the line and M_R is the radiating ion mass. Some values of FWHM $\hbar\omega_w$ for aluminum are shown in Table I. Finally, we fold to account for the experimental resolution.

We discuss now the simulated Ly _{α} -line profiles at solid state densities $n_0 \leq n_e \leq 4n_0$, where $n_0 = 5 \times 10^{23}$ cm⁻³ and $k_B T = 500$ eV. Some results for the Ly _{α} -line shape without Doppler broadening and LS coupling are shown in Figs. 2-4. In all cases the ratio $a_Z/a \ll 1$ is small and the use of the dipole approximation in Eq. (7) is fulfilled. The line broadening and shift towards lower photon energies (redshift) is clearly visible in Fig. 2, which shows the line profile at fixed temperature 500 eV and different densities. Here the parameters δ_{ei} , δ_{ee} and δ_{ii} are determined as the thermal wavelengths. With increasing density the influence of the plasma effects on the line shape becomes more pronounced. At very large densities from $n_e = 2.6n_0$ (green line) and up to the value $n_e = 4n_0$ (blue line) there is hardly any broadening and the line is only redshifted towards lower photon energies by the plasma effects. In this high density regime the fluctuating electric fields become sufficiently strong to cause asymmetric shapes due to nonlinear coupling.

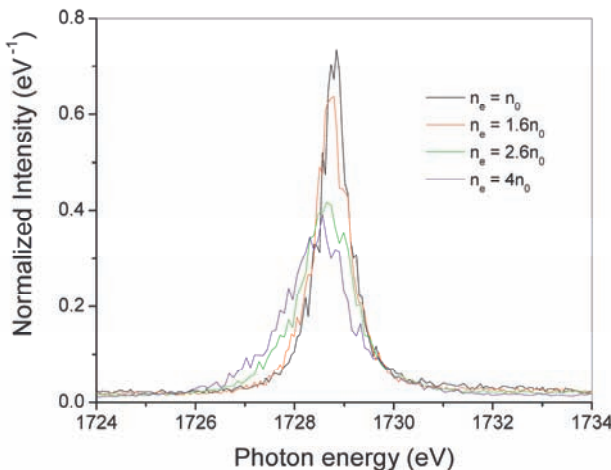


FIG. 2: Simulated Ly _{α} -spectra of a Al^{12+} radiating ion embedded in an Al^{13+} -TCP of a temperature of 500 eV and solid state density $n_e = n_0$ (black line), $n_e = 1.6n_0$ (red line), $n_e = 2.6n_0$ (green line) and $n_e = 4n_0$ (blue line). The spectra are normalized to the area under curves.

To gain more insight we now fix the plasma temperature (500 eV) and the density ($n_e = n_0$) and show in Fig. 3 the line profile for different regularization parameters $\delta = \delta_{ei}$ (the lines without symbols), $\delta = 0.08a$ (blue), $\delta = 0.1a$ (red) and $\delta = 0.4a$ (green). On the right the thermal wavelengths of the electrons are chosen as the relevant lengths δ at which a smoothening of the ion-electron interaction due to quantum diffraction becomes effective. For comparison we also calculate the line shapes for non-isothermal plasma with different electronic and ionic temperatures $T_e = 500$ eV and $T_i = 50$ eV, respectively (the lines with symbols). As shown in Fig. 3 the width of the lines decreases with increasing parameter δ , i.e. by 'softening' of the ion-electron interaction. Besides, keeping the electron temperature unchanged and decreasing the ionic temperature leads to an additional broadening of the lines and this is visible for more Coulomb-like interactions with small δ .

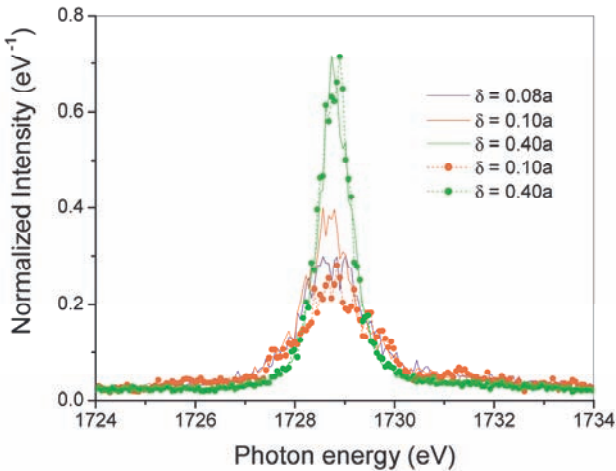


FIG. 3: Simulated Ly _{α} -spectra of a Al¹²⁺ radiating ion embedded in an Al¹³⁺-TCP of a density $n_e=n_0$. The lines without and with symbols correspond to the equilibrium ($T_e=T_i=500$ eV) and non-equilibrium ($T_e=500$ eV, $T_i=50$ eV) TCPs, respectively. The regularization parameters is $d=0.08a$ (blue line), $d=0.1a$ (red line) and $d=0.4a$ (green line). The spectra are normalized to the area under the curves.

In Fig. 4 we put together the results obtained for two values of plasma densities (n_0 and $2n_0$) and the parameter δ . In the top and bottom panels we take $\delta = 1.5a_Z$ and $\delta = 7.6a_Z$, respectively, where a_Z is the effective Bohr radius of Al¹²⁺. Note that for two plasma densities n_0 and $2n_0$ the chosen values of δ in units of a_Z are equivalent to 0.08a, 0.1a and 0.4a, 0.5a, respectively, in units of the Wigner-Seitz radius a of a TCP. Thus the plasma parameters here are the same as in Fig. 1. As we have done in Fig. 1 we also demonstrate the influence of the electron-ion attractive interaction on the spectral line shapes plotting the spectra $I_0(\omega)$ resulting from a superposition of the electronic and ionic OCPs (red lines). $I_0(\omega)$ is calculated by folding the spectra $I_e(\omega)$ and $I_i(\omega)$ which are obtained from simulations of the radiative transitions of a radiator embedded in an electronic OCP and of the ionic OCP, respectively. The microfields $E(t)$ in an electronic and ionic OCPs are simulated at a neutral and charged reference points, respectively. The spectrum $I_0(\omega)$ thus represents the line shape in a TCP assuming that the ion-electron attractive interaction is switched off. As shown in Fig. 4 the width of the line now turns out to be highly sensitive to both the choice of δ and the density n_e , with a much stronger dependence on n_e for smaller δ . The influence of the high-electric field tails in the MFDs at small δ (see Fig. 1) on the spectral lines is now clearly shown in Fig. 4. Smaller δ results in higher electric fields which broaden the spectral lines and reduce the peak intensity. More precisely we observed that the line width behaves approximately as $\hbar\Delta\omega \sim n_e/\delta$.

In the following we will compare our calculations with the results of experiments performed in Garching [16] where an Al plasma is created by the irradiation of the target with laser pulses of 150 fs duration at an intensity of a few 10^{17} W/cm². The systematic investigations carried out in Refs. [17, 18] show that the standard (quasistatic and impact) approximations become doubtful if the plasma density reaches that of the solid state. In the last years experiments have approached this regime, see, e.g., [14–

16]. We note that the theoretical model discussed so far assumes homogeneous equilibrium plasma. Obviously this is not the state in which the laser leaves the target after the irradiating pulse. In particular, self-absorption due to plasma inhomogeneities leads to an additional line broadening which is difficult to analyze. Fortunately there has been considerable experimental progress to reduce the self-absorption [16].

Earlier experiments on the Ly _{α} -line in Al¹²⁺ at solid state density [14, 15] were subject to self-absorption in the cooler and less dense surface regions of the target. This can be prevented by using thin (to reduce absorption) target layers with sharp boundaries (to enhance homogeneity). For that purpose a 25 nm Al target layer was embedded in solid carbon at depths ranging from $d = 25$ nm to $d = 400$ nm [16]. With increasing depth the expansion of the Al layer is suppressed and the homogeneity of the Al plasma is improved. In Fig. 5 we compare our simulations with the experimental results (blue circles) for $d = 400$ nm and $k_B T = 500$ eV from which the underground has been subtracted. The fine structure and the Doppler broadening are taken into account as described above. Then the simulated Ly _{α} -lines are folded with the experimental resolution (0.9 eV, FWHM) and compared with the experimental line assuming densities 5×10^{23} cm⁻³ (red line) and 10^{24} cm⁻³ (green line). At these two densities the plasma parameters for the Al¹³⁺-TCP are $\Gamma_{ii} = 2.65$, $\Gamma_{ee} = 0.04$ and $\Gamma_{ie} = 3.34$, $\Gamma_{ee} = 0.05$, respectively. All curves in Fig. 5 are normalized to the peak intensity. Finally, the position of the simulated line must be redshifted by 2 eV. This is the dense plasma line shift (DPLS) Ref. [7] due to the screening of the electron-nucleus interaction by hot background electrons which is not yet included in our simulations. Assuming a Debye-screened interaction instead of the r^{-1} -Coulomb potential first-order perturbation theory yields a shift of the required magnitude. A comparison of the two simulated curves in Fig. 5 allows concluding that the remaining uncertainty in the determination of the density of the target is of the order of 10^{23} cm⁻³. Our results show that the quantum mechanics of close electron-ion collisions is important over and above the plasma redshift. If the quantum diffraction parameter δ is fixed at physically reasonable values near the effective Bohr radius a_Z , our calculations favor a somewhat larger density than n_0 as proposed in Ref. [16]. Clearly a more quantum mechanical treatment of the electron component in the plasmas is desirable.

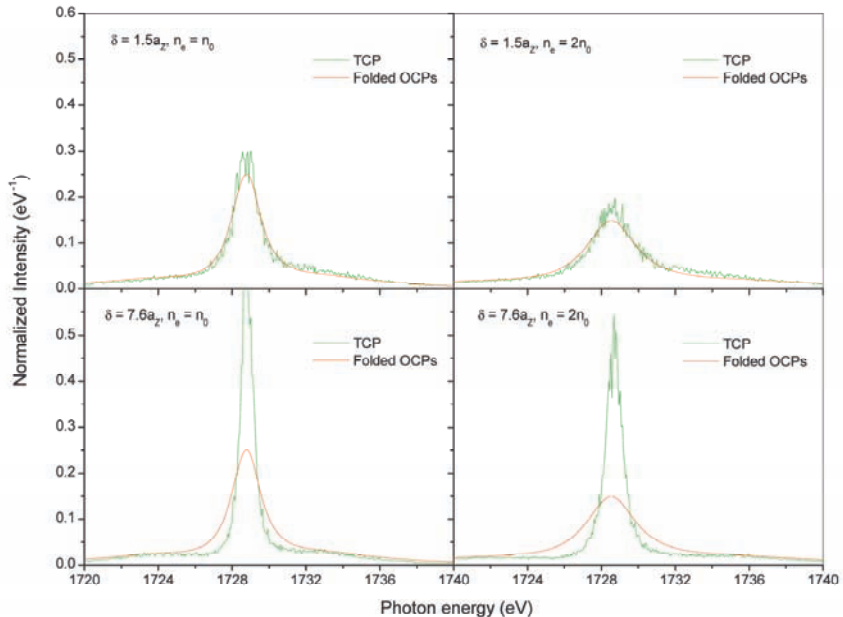


FIG. 4: Simulated Ly _{α} -spectra of a Al¹²⁺ radiating ion embedded in a Al¹³⁺-TCP (green) of a temperature of 500 eV and solid state densities $n_e = n_0$ (left panels) and $n_e = 2n_0$ (right panels). The spectra are normalized to the area under the curves. The parameter δ is $1.5a_Z$ and $7.6a_Z$ in the top and bottom panels, respectively. The red lines are the spectra obtained from the folding of an electronic and an ionic OCP.

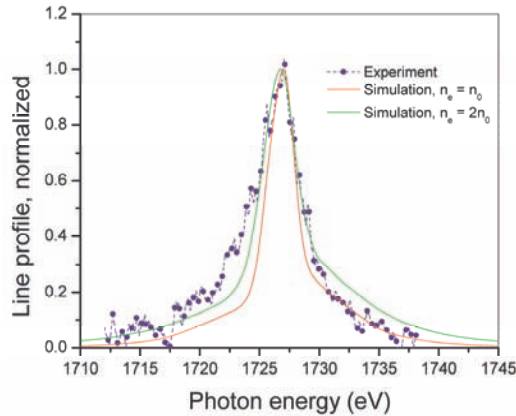


FIG. 5: Comparison of the experimental line [16] (blue circles) with our simulation results (red and green lines), i.e. with the green curves from the top panels of Fig. 4 after taking into account the Doppler broadening, the LS-coupling, the experimental resolution and a redshift (see text). The experimental line is subtracted by the underground. Here the curves are normalized to the peak intensity.

V. CONCLUSIONS

In this paper we have presented a model for spectral lines that works without some assumptions which underly the conventional impact and quasi-static approximations. In particular we (i) consider two-component plasma (TCP) with attractive interactions between electrons and ions, (ii) account for the strong Coulomb correlations between plasma particles, (iii) account for radiator states including the continuum, which are not directly involved in the transition, (iv) allow for a nonperturbative treatment. Our simulations cover a wide range in the densitytemperature plane where the impact and quasi-static approximations become doubtful or even fail. We have compared our model with recent experiments on Al targets and found good agreement for the Ly α -transitions. The more exact treatments beyond the traditional approximations will become highly desirable in connection with experiments at higher densities and temperatures at the planned (X)FEL facilities. A critical discussion of our results suggests further improvements. (i) The dipole approximation in Eq. (7) for the interaction of the microfield with the radiator suffices for the present experiments [16]. In even denser plasmas one must account for close collisions between the radiator and the plasma particles with a quadrupole term in the expansion of the interaction and finally with an exact treatment [11]. In this connection we note that the electron-ion interaction has been studied recently by MD simulations and in theoretical models like the hypernetted-chain-approximation (HNC) [19–21, 23]. (ii) Relativistic and spin effects beyond the simple fine structure given by Eq. (9) can be taken into account by treating the radiator with the Dirac equation [30]. (iii) The major He-like satellite is well separated from the Ly α -line in the experiment [16]. However, there will be closer satellites due to spectator electrons in higher configurations, which may affect the 'red' shoulder of the line. For spectators in the continuum this effect merges into the DPLS. The satellites impose a challenge as they offer an additional tool to determine the temperature of the plasma, see, e.g., Ref. [35]. For that purpose one has to solve the multi-electron wave equation, for example in the relativistic case the Dirac equation [36].

ACKNOWLEDGMENTS

The work of H.B. Nersisyan and C. Toepffer was supported by the Deutsche Forschungsgemeinschaft (DFG TO 91/5-3), the Bundesministerium für Bildung und Forschung (BMBF, 06ER128) and by the Gesellschaft für Schwerionenforschung (GSI, ER/TOE). The work of H.H. Matevosyan was supported by International Science and Technology Center (ISTC) Project No. A-1307.

- [1] G. A. Mourou, C. P. J. Barty, M. D. Perry, Phys. Today 51, 22 (1998).
- [2] E. M. Campbell, W. J. Hogan, D. H. Crandall, C. R. Acad. Sci. Paris 1, Série IV, 671 (2000).
- [3] R. Ramis et al., Nucl. Instr. Meth. A 464, 45 (2001).
- [4] P. M. Celliers et al, Phys. Rev. Lett. 84, 5564 (2000).
- [5] R. Redmer, Phys. Rep. 282, 35 (1997).
- [6] D. Saumon et al., Astrophys. J. 391, 827 (1992).
- [7] R. Griem, Spectral Line Broadening in Plasmas (Academic Press, New York, 1974).
- [8] C. A. Iglesias, J. L. Lebowitz, D. MacGowan, Phys. Rev. A 28, 1667 (1983).
- [9] J. W. Dufty, D. B. Boercker, C. A. Iglesias, Phys. Rev. A 31, 1681 (1985).
- [10] D. B. Boercker, C. A. Iglesias, J. W. Dufty, Phys. Rev. A 36, 2254 (1987).
- [11] G. C. Junkel, M. A. Gunderson, C. F. Hooper Jr., Phys. Rev. E 62, 5584 (2000).
- [12] D. A. Haynes et al., Phys. Rev. E 53, 1042 (1996).
- [13] S. P. Regan et al., Phys. Plasmas 9, 1357 (2002).
- [14] A. Saemann et al., Phys. Rev. Lett. 82, 4843 (1999).
- [15] K. Eidmann et al., J. Quant. Spectrosc. Radiat. Transfer 65, 173 (2000).
- [16] U. Andiel et al., Europhys. Lett. 60, 861 (2002).
- [17] J. Marten, thesis, Erlangen University, Erlangen (2003).
- [18] J. Marten and C. Toepffer, Eur. Phys. J. D 29, 397 (2004).
- [19] H. B. Nersisyan, C. Toepffer, G. Zwicknagel, Phys. Rev. 9, E 72, 036403 (2005).
- [20] H. B. Nersisyan, G. Zwicknagel, J. Phys. A: Math. and General 39, 4677 (2006).
- [21] H. B. Nersisyan, D. A. Osipyan, and G. Zwicknagel, Phys. Rev. E 77, 056409 (2008).
- [22] T. Morita, Prog. Theor. Phys. 22, 757 (1959); ibid 23, 1211 (1960).
- [23] B. Talin, A. Calisti, J. Dufty, Phys. Rev. E 65, 056406 (2002).
- [24] G. Kelbg, Ann. Phys. (Leipzig) 12, 219 (1963); ibid 13, 354 (1964); ibid 14, 394 (1964).
- [25] C. Deutsch, Y. Furutani, M. M. Gombert, Phys. Rep. 69, 85 (1981); C. Deutsch, Phys. Lett. A 60, 317 (1970); C. Deutsch, M.-M. Gombert, H. Minoo, Phys. Lett. A 66, 381 (1978); H. Minoo, M.-M. Gombert, C. Deutsch, Phys. Rev. A 23, 924 (1981).
- [26] J. Holtsmark, Ann. Phys. 58, 577 (1919).
- [27] C. F. Hooper Jr., Phys. Rev. 165, 215 (1968).
- [28] H. Mayer, Los Alamos Scientific Report LA-647 (1947).
- [29] G. Zwicknagel, C. Toepffer, P.-G. Reinhard, Phys. Rep. 309, 117 (1999).
- [30] U. Müller-Nehler and G. Soff, Phys. Rep. 246, 101 (1994).
- [31] F. Calvayrac et al., Phys. Rep. 337, 493 (2000).
- [32] E.-M. Reinecke, thesis, Erlangen University, Erlangen (2000).
- [33] H. Friedrich, Theoretical Atomic Physics (Springer, Berlin, 1990).
- [34] J. D. Jackson, Classical Electrodynamics (John Wiley, New York, 1998).
- [35] D. Salzmann, Atomic Physics in Hot Plasmas (Oxford University Press, New York, 1998).
- [36] K. G. Dyall et al., Comput. Phys. Commun. 55, 425 (1989).